

Euler State Networks: Non-dissipative Reservoir Computing

Claudio Gallicchio

*University of Pisa, Department of Computer Science
Largo Bruno Pontecorvo, 3, Pisa, 56127, Italy*

Abstract

Inspired by the numerical solution of ordinary differential equations, in this paper we propose a novel Reservoir Computing (RC) model, called the Euler State Network (EuSN). The introduced approach makes use of forward Euler discretization and antisymmetric recurrent matrices to design reservoir dynamics that are both stable and non-dissipative by construction.

Our mathematical analysis shows that the resulting model is biased towards unitary effective spectral radius and zero local Lyapunov exponents, intrinsically operating at the edge of stability. Experiments on synthetic tasks indicate the marked superiority of the proposed approach, compared to standard RC models, in tasks requiring long-term memorization skills. Furthermore, results on real-world time series classification benchmarks point out that EuSN is capable of matching (or even surpassing) the level of accuracy of trainable Recurrent Neural Networks, while allowing up to 100-fold savings in computation time and energy consumption.

Keywords: Reservoir Computing, Echo State Networks, Recurrent Neural Networks, Stable Neural Architectures

1. Introduction

The interest in studying neural network architectures from a dynamical system perspective has recently been attracting increasing research attention [1, 2, 3, 4]. The key insight is that the computation performed by some kinds of neural networks, e.g., residual networks, can be understood as the numerical solution to an ordinary differential equation (ODE) through discretization [5]. This intuitively simple observation brings about the possibility of imposing desirable properties in the behavior of the neural network by imposing specific conditions to the corresponding ODE. Stability plays a key role in this sense, being related to the propagation of both input signals, during inference, and gradients, during training.

In this paper, we focus on Recurrent Neural Network (RNN) architectures, and especially on Reservoir Computing (RC) [6, 7]. RC establishes a particularly attractive approach for the design and training of RNNs, where the hidden recurrent *reservoir* layer

Email address: gallicch@di.unipi.it (Claudio Gallicchio)

Preprint submitted to Journal

is left untrained, leaving the entire training effort to the output layer alone. The stability of forward signal propagation through the reservoir is therefore of great importance. Due to the fact that the parameters that determine the dynamics of the reservoir are untrained, some form of constraint is indeed necessary to avoid instability when the network is operated with a driving input. This aspect is related to the widely known fading memory property of RC networks, which makes it difficult to maintain the input signal information in the state dynamics across several time-steps. Although this limitation, RC has become more and more popular because of the impressively advantageous trade-off between predictive performance and training efficiency. As a result, it is often the chosen approach for embedded applications distributed at the edge [8, 9], as well as for RNN implementations in neuromorphic hardware [10, 11, 12]. However, the performance gap with fully trainable state-of-the-art RNNs still leaves space for improvements.

This paper extends our previous work in [13], introducing and analyzing a new RC method that is inspired by the numerical solution of ODEs. As the reservoir architecture is obtained by forward Euler discretization of an intrinsically stable ODE, the resulting model is called the Euler State Network (EuSN). The initialization condition imposed to the reservoir inherently yields state dynamics that are biased to be both stable and non-dissipative, thereby mitigating the lossy transmission of input signals over time, sensibly reducing the performance gap with fully trainable RNNs in time-series classification tasks.

The contributions of this work can be summarized as follows:

- We introduce the EuSN model, a novel approach to design RC neural network architectures based on ODE discretization. Overcoming the natural limitations of standard RC models, EuSN is specifically designed to fulfill both stability and non-dissipative properties.
- We derive a mathematical characterization of the proposed reservoir system, focusing on its asymptotic stability and local Lyapunov exponents.
- We provide an extensive experimental evaluation of EuSN. First, we shed light on its long-term memorization abilities in comparison to standard RC models. Then, we assess the accuracy-efficiency trade-off of EuSN in comparison to both RC and fully trainable RNN models on several time-series classification benchmarks.

The rest of this paper is organized as follows. In Section 2 we give an overview on the basic concepts of RC. We introduce the EuSN model in Section 3, and we elaborate its mathematical analysis in Section 4. The experimental assessment of the approach is provided in Section 5. Finally, Section 6 concludes the paper.

2. Reservoir Computing and Echo State Networks

Reservoir Computing (RC) is a common denomination for a class of recurrent neural models that are based on untrained internal dynamics [6, 7, 10]. In general, the architecture comprises a fixed hidden recurrent layer called *reservoir*, and an output *readout* layer that is the only trainable component. Here, in particular, we focus on the Echo State Network (ESN) model [14, 15], where the reservoir operates in discrete time-steps and typically makes use of tanh non-linearity. We consider a reservoir architecture with

N reservoir neurons and X input units, using $\mathbf{h}(t)$ and $\mathbf{x}(t)$ to denote, respectively, the state of the reservoir and the external input at time-step t . Referring to the general ESN formulation with leaky integrator neurons [16], the reservoir state is evolved according to the following iterated map:

$$\mathbf{h}(t) = (1 - \alpha) \mathbf{h}(t - 1) + \alpha \tanh(\mathbf{W}_h \mathbf{h}(t) + \mathbf{W}_x \mathbf{x}(t) + \mathbf{b}), \quad (1)$$

where $\alpha \in (0, 1]$ is the leaking rate, $\mathbf{W}_h \in \mathbb{R}^{N \times N}$ is the recurrent reservoir weight matrix, $\mathbf{W}_x \in \mathbb{R}^{N \times X}$ is the input weight matrix, and $\mathbf{b} \in \mathbb{R}^N$ is a vector of bias weights. As an initial condition, the reservoir state is typically started at the origin, i.e., the null vector: $\mathbf{h}(0) = \mathbf{0}$.

Interestingly, all the weight values that parametrize the behavior of the reservoir, i.e., the values in \mathbf{W}_h , \mathbf{W}_x and \mathbf{b} can be left untrained provided that the state dynamics satisfy a global asymptotic stability property called the Echo State Property (ESP) [17, 15]. Essentially, the ESP states that when driven by a long input time-series, reservoir dynamics tend to synchronize [18] irrespectively of initial conditions, whose influence on the state progressively fade away. Tailoring the reservoir initialization to the properties of the input signal and task still represents a challenging theoretical research question [19, 20]. However, in RC practice, it is common to follow a simple initialization process linked to a necessary condition for the ESP [7, 15, 21]. The recurrent reservoir weight matrix \mathbf{W}_h is initialized randomly, e.g., from a uniform distribution over $[-1, 1]$, and then re-scaled to limit its spectral radius $\rho(\mathbf{W}_h)$ to a value smaller than 1. Notice that this would require computing the eigenvalues of potentially large matrices, and thereby might result in a computationally demanding process. A more convenient procedure, in this case, can be obtained by using the circular law from random matrix theory, as illustrated in [22]. The weight values in \mathbf{W}_x and \mathbf{b} are randomly drawn from a uniform distribution over $[-\omega_x, \omega_x]$ and $[-\omega_b, \omega_b]$, respectively. The values of α , $\rho(\mathbf{W}_h)$, ω_x and ω_b are treated as hyper-parameters.

The trainable readout can be implemented in several forms. In this paper, we focus on classification tasks and use a dense output layer that is fed by the last state computed by the reservoir when run on an input time-series.

ESP limitations – Regarding the ESP, it is worth noticing that while enabling a stable encoding robust to input perturbations, the required stability property gives a fading memory structure to the reservoir dynamics. As shown in [23], the reservoir state space tends to organize in a suffix-based fashion, in agreement with the architectural Markovian bias of contractive RNNs [24, 25]. On the one hand, this means that ESNs are particularly well suited to solve tasks defined in compliance with this characterization, i.e., where the information in the suffix of the input time-series is dominant in determining the output [23]. On the other hand, reservoir dynamics are constrained to progressively forget previous stimuli, making it difficult to propagate input information efficiently through many time-steps, as is required for example in classification tasks.

Ring Reservoirs – While randomization plays an important role in RC, several studies in literature tried to find reservoir organizations that perform better than just random ones. A fruitful line of research deals with constraining the reservoir topology [26] to get desirable algebraic properties of the recurrent weight matrix \mathbf{W}_h , especially based

on an orthogonal structure [27, 28]. A simple yet effective way to achieve this goal consists in shaping the reservoir topology such that the reservoir neurons are arranged to form a cycle, or a *ring*. This specific architectural variant of ESNs has been shown to have noticeable advantages, e.g., in terms of the richness of the developed dynamics, longer memory, and performance on non-linear tasks [29, 30, 31]. In this paper, we thereby consider ESN based on ring reservoirs (R-ESN) as a competitive alternative to the standard vanilla setup.

3. The Euler State Network Model

To introduce the proposed model, we start by considering the operation of a continuous-time recurrent neural system modeled by the following ODE:

$$\begin{aligned} \mathbf{h}'(t) &= f(\mathbf{h}(t), \mathbf{x}(t)) \\ &= \tanh(\mathbf{W}_h \mathbf{h}(t) + \mathbf{W}_x \mathbf{x}(t) + \mathbf{b}) \end{aligned} \tag{2}$$

where $\mathbf{h}(t) \in \mathbb{R}^N$ and $\mathbf{x}(t) \in \mathbb{R}^X$ respectively denote the state and the driving input, $\mathbf{W}_h \in \mathbb{R}^{N \times N}$ is the recurrent weight matrix, $\mathbf{W}_x \in \mathbb{R}^{N \times X}$ is the input weight matrix, and $\mathbf{b} \in \mathbb{R}^N$ is the bias.

We are interested in applying two types of constraints to the system in eq. 2, namely *stability* and *non-dissipativity*. The former is required to develop a robust information processing system across time-steps, avoiding explosion of input perturbations that would result in poor generalization. The latter is important to avoid developing lossy dynamics, which would determine catastrophic forgetting of past inputs during the state evolution.

We recall that the solution to an ODE is stable if the real part of all eigenvalues of the corresponding Jacobian are ≤ 0 . Denoting the Jacobian of the system in eq 2 as $\mathbf{J}_f(\mathbf{h}(t), \mathbf{x}(t))$, and using $\lambda_i(\cdot)$ to indicate the i -th eigenvalue of its matrix argument, the stability constraint in our case can be expressed as

$$\max_i \operatorname{Re}(\lambda_i(\mathbf{J}_f(\mathbf{h}(t), \mathbf{x}(t)))) \leq 0. \tag{3}$$

On the other hand, if the real parts of these eigenvalues are $\ll 0$, then the resulting dynamics are lossy. We thereby seek for a critical condition under which the eigenvalues of the Jacobian of our ODE are featured by ≈ 0 real parts, i.e.:

$$\operatorname{Re}(\lambda_i(\mathbf{J}_f(\mathbf{h}(t), \mathbf{x}(t)))) \approx 0 \quad i = 1, \dots, N. \tag{4}$$

A rather simple way to meet the condition in eq 4 is to require that the recurrent weight matrix \mathbf{W}_h is antisymmetric [5], i.e., it satisfies

$$\mathbf{W}_h = -\mathbf{W}_h^T. \tag{5}$$

In fact, in this case the eigenvalues of \mathbf{W}_h , and consequently those of the Jacobian $\mathbf{J}_f(\mathbf{h}(t), \mathbf{x}(t))$ are all purely imaginary (see, e.g., [32] for a proof). Crucially, this property is *intrinsic* to the antisymmetric structure imposed to the recurrent weight matrix \mathbf{W}_h , irrespectively of the particular choice of its values. In other words, the targeted critical dynamical behavior can be seen as an *architectural bias* of the neural system described

by eq. 2 under the imposed antisymmetric constraint in eq. 5. Taking an RC perspective, we can then leave all the weight values in eq 2, i.e., \mathbf{W}_h , \mathbf{W}_x and \mathbf{b} , *untrained*, provided that eq. 5 is satisfied.

Finally, to develop our discrete-time reservoir dynamics, we note that the ODE in eq. 2 can be solved numerically by using the forward Euler method [33], resulting in the following discretization:

$$\begin{aligned} \mathbf{h}(t) &= F(\mathbf{h}(t-1), \mathbf{x}(t)) \\ &= \mathbf{h}(t-1) + \varepsilon \tanh\left((\mathbf{W}_h - \gamma\mathbf{I})\mathbf{h}(t-1) + \mathbf{W}_x\mathbf{x}(t) + \mathbf{b}\right), \end{aligned} \tag{6}$$

where ε is the step size of integration, and γ is a diffusion coefficient used for stabilizing the discrete forward propagation [5]. Note that both ε and γ are typically small positive scalars, and are treated as hyper-parameters. We can now look at eq. 6 as the state transition equation of a discrete-time *reservoir* layer with N recurrent neurons and X input units, where \mathbf{W}_h , \mathbf{W}_x and \mathbf{b} are untrained, and \mathbf{W}_h satisfies the constraint of being antisymmetric in eq. 5. Since the untrained reservoir dynamics evolves as the forward Euler solution to an ODE, we call the resulting model *Euler State Network* (EuSN). As in standard RC/ESN, the reservoir state is initialized at the origin, i.e., $\mathbf{h}(0) = \mathbf{0}$. Moreover, the reservoir feeds a *readout* layer, which is the only trained component of the EuSN architecture.

To *initialize* the reservoir, we propose the following simple procedure, analogous to the common approaches in RC literature:

- To setup the recurrent weights, we start by randomly initializing the values of a matrix $\mathbf{W} \in \mathbb{R}^{N \times N}$ from a uniform distribution over $[-\omega_r, \omega_r]$, where ω_r is a positive *recurrent scaling* coefficient. We then set $\mathbf{W}_h = \mathbf{W} - \mathbf{W}^T$, which satisfies eq. 5 as it is antisymmetric by construction.
- The values of the input weight matrix \mathbf{W}_x are randomly initialized from a uniform distribution over $[-\omega_x, \omega_x]$, where ω_x is a positive *input scaling coefficient* as in ESNs.
- The values of the bias vector \mathbf{b} are randomly initialized from a uniform distribution over $[-\omega_b, \omega_b]$, where ω_b is a positive *bias scaling coefficient* as in ESNs.

Notice that the stability properties of the reservoir are due to the antisymmetric structure of \mathbf{W}_h , without requiring to scale its spectral radius as in ESNs. The recurrent, input and bias scaling coefficients ω_r , ω_x , and ω_b , are introduced simply to balance the contributions of the different terms in the state transition eq. 6, and are treated as hyper-parameters.

It is worth mentioning that, in the broader landscape of trainable RNN research, the introduced EuSN model brings similarities to the Antisymmetric RNN (A-RNN) [32], which is featured by state dynamics evolving as in eq. 6, under a similar antisymmetric constraint on the recurrent weight matrix. Crucially, while in EuSN all the internal weights are left untrained after initialization, in A-RNN they are all trainable. In this view, the study of EuSN can be seen under the perspective of randomized neural networks [34], emphasizing the intrinsic capabilities of stable recurrent architectures based on

forward Euler discretization and antisymmetric recurrent weight matrices even in the absence (or prior to) training of internal connections.

The following Section 4 delves into the mathematical analysis of the EuSN reservoir system, studying its asymptotic stability properties and its intrinsically critical dynamical regime.

4. Mathematical Analysis

We study the reservoir of an EuSN as a discrete-time dynamical system evolving according to the function F defined in eq. 6, where we remind that \mathbf{W}_h is antisymmetric, and both ε and γ are small positive reals. The local behavior of the reservoir system around a specific state \mathbf{h}_0 can be analyzed by linearization, i.e., by approximating its dynamics as follows:

$$\mathbf{h}(t) = \mathbf{J}_F(\mathbf{h}_0, \mathbf{x}(t)) (\mathbf{h}(t-1) - \mathbf{h}_0) + F(\mathbf{h}_0, \mathbf{x}(t)). \quad (7)$$

Here $\mathbf{J}_F(\mathbf{h}_0, \mathbf{x}(t))$ is used to denote the Jacobian of the function F in eq. 6 at time-step t and evaluated at \mathbf{h}_0 , i.e.:

$$\mathbf{J}_F(\mathbf{h}_0, \mathbf{x}(t)) = \left. \frac{\partial F(\mathbf{h}(t-1), \mathbf{x}(t))}{\partial \mathbf{h}(t-1)} \right|_{\mathbf{h}=\mathbf{h}_0}. \quad (8)$$

In classical ESN literature it is common to study the eigenspectrum of the Jacobian of the reservoir, and especially its spectral radius, in order to characterize the asymptotic stability behavior of the system. In particular, when introducing necessary conditions for the ESP [15], it is common to study the autonomous system (i.e., in the absence of driving input $\mathbf{x}(t) = \mathbf{0}$ for every t , and bias $\mathbf{b} = \mathbf{0}$), linearized around the origin (i.e., $\mathbf{h}_0 = \mathbf{0}$). For ESNs, this procedure then results in an algebraic constraint that is imposed on the recurrent weight matrix of the reservoir in order to control its effective spectral radius. Interestingly, by taking the same assumptions in the case of EuSN, we find that all the eigenvalues of the Jacobian are naturally confined to a neighborhood of 1. This result is stated by the following Proposition 1, where we use the notation $\lambda_i(\cdot)$ to indicate the i -th eigenvalue of its argument.

Proposition 1. *Let us consider an EuSN whose reservoir dynamics are ruled by the state transition function in eq. 6, where both ε and γ are small positive scalars. Assume autonomous (i.e., with null driving input and bias) and linearized dynamics around the origin. Then, the eigenvalues of the resulting Jacobian satisfy the following condition:*

$$\lambda_i(\mathbf{J}_F(\mathbf{0}, \mathbf{0})) \approx 1 \quad i = 1, \dots, N. \quad (9)$$

Proof. Computing an expression for the Jacobian in eq. 8 around the origin and in the absence of external input, we find that:

$$\mathbf{J}_F(\mathbf{0}, \mathbf{0}) = \mathbf{I} + \varepsilon(\mathbf{W}_h - \gamma\mathbf{I}) = \mathbf{I}(1 - \varepsilon\gamma) + \varepsilon\mathbf{W}_h. \quad (10)$$

We can notice that each eigenvalue of the sum of matrices in the right-hand side of eq. 10 is given by an eigenvalue of $\mathbf{I}(1 - \varepsilon\gamma)$ added to an eigenvalue of $\varepsilon\mathbf{W}_h$, i.e.:

$$\lambda_i(\mathbf{J}_F(\mathbf{0}, \mathbf{0})) = 1 - \varepsilon\gamma + \varepsilon\lambda_i(\mathbf{W}_h) \quad i = 1, \dots, N. \quad (11)$$

The result then follows straightforwardly by recalling that ε and γ are both small positive values, hence the expression in the right-hand side of eq. 11 is dominated by 1. \square

Proposition 1 has interesting consequences in terms of the asymptotic behavior of the reservoir. Indeed, as all the eigenvalues of the Jacobian $\mathbf{J}_F(\mathbf{0}, \mathbf{0})$ are ≈ 1 , it follows that the autonomous operation of the reservoir system around the origin tends to preserve all the components of the state, while performing infinitesimal rotations due to the antisymmetric structure of the recurrent matrix. Any perturbation to the zero state (i.e., of the origin) is preserved over time without vanishing, which essentially means that EuSNs do not tend to show the ESP under the proposed initialization conditions. The qualitative difference between the behaviors of an EuSN and those of an ESN is graphically illustrated in Figure 1. In the figure, taking inspiration from the graphical analysis of the inner dynamics of deep architectures used in [5] and [32], we visualize examples of state trajectories developed by 2-dimensional autonomous reservoirs in different conditions: ESN with and without ESP, R-ESN with orthogonal weight matrix, and EuSN. In the case of ESNs, when the ESP is valid (Figure 1a), the origin is an attractor and all the trajectories quickly converge to it. When instead the ESN does not satisfy the ESP (Figure 1b), the origin is a repeller. In the case of R-ESN (Figure 1c), even if the recurrent weight matrix is orthogonal, trajectories still converge to the origin (more slowly than in Figure 1a) due to contractive properties of the tanh non-linearity. Interestingly, in the case of EuSN (Figure 1d), the states rotate around the origin without being attracted nor repelled, and the distance between the orbits are preserved, reflecting the differences among the initial conditions. In other words¹, differently from ESN variants, the effect of the external input on the reservoir dynamics in EuSN does not die out nor explode with time.

A closer inspection of eq. 11 also reveals that the small deviations from 1 in the eigenvalues of the Jacobian in $\mathbf{J}_F(\mathbf{0}, \mathbf{0})$ are possibly due to the combined effects of the actual values of ε , γ , and of the leading eigenvalue of the recurrent reservoir weight matrix \mathbf{W}_h . In this case, it is also possible to derive a simple and direct expression for the effective spectral radius of the autonomous linearized EuSN system, as given by the following Corollary 1.

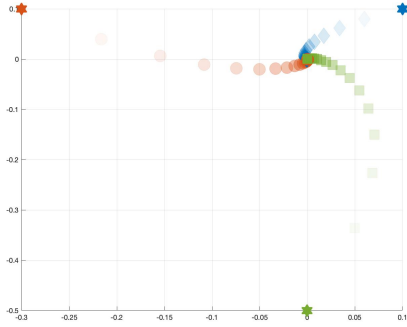
Corollary 1. *Let us consider an EuSN whose reservoir dynamics are ruled by the state transition function in eq. 6, where both ε and γ are small positive scalars. Assume autonomous (i.e., with null driving input and bias) and linearized dynamics around the origin. The spectral radius of the resulting Jacobian is then given by the following expression:*

$$\rho(\mathbf{J}_F(\mathbf{0}, \mathbf{0})) = \sqrt{1 + \varepsilon^2 \gamma^2 - 2\varepsilon\gamma + \varepsilon^2 \rho(\mathbf{W}_h)^2}, \quad (12)$$

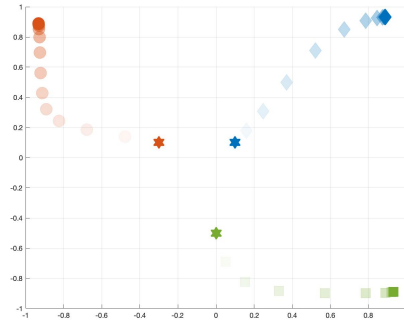
where $\rho(\mathbf{W}_h)$ denotes the spectral radius of the reservoir weight matrix.

Proof. Due to its antisymmetric structure, the eigenvalues of \mathbf{W}_h are all purely imaginary, i.e., they are in the form $\lambda_i(\mathbf{W}_h) = \iota b_i$ for all $i = 1, \dots, N$. Hence, we can express the spectral radius of \mathbf{W}_h as $\rho(\mathbf{W}_h) = \max_i |b_i|$. Then, the statement directly follows by

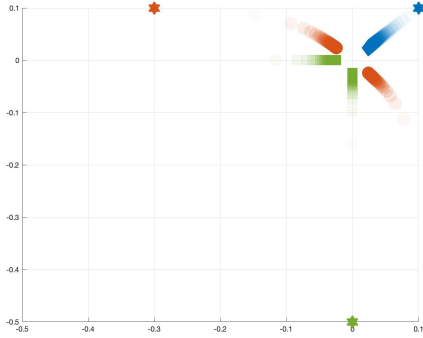
¹The different initial conditions can be interpreted as the same reservoir state perturbed by different external input values.



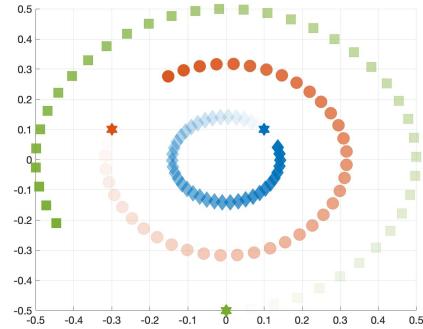
(a) ESN with ESP.



(b) ESN without ESP.



(c) R-ESN.



(d) EuSN.

Figure 1: Autonomous reservoir dynamics around the origin visualized for instances of: (a) ESN with ESP, (b) ESN without ESP, (c) R-ESN, and (d) EuSN. The same three initial conditions are used in all the cases, illustrated as full stars of different colors: $\mathbf{u}_0 = [0.1, 0.1]^T$ in blue, $\mathbf{v}_0 = [-0.3, 0.1]^T$ in red, and $\mathbf{z}_0 = [0, -0.5]^T$ in green. Trajectories in the 2-dimensional reservoir space are shown by (sampled) points of different shapes, where more transparent colors indicate earlier time-steps. The recurrent weight matrix is: $\mathbf{W}_h = \begin{bmatrix} 0.7 & 0.1 \\ -0.1 & 0.7 \end{bmatrix}$ in (a); $\mathbf{W}_h = \begin{bmatrix} 1.7 & 0.1 \\ -0.1 & 1.7 \end{bmatrix}$ in (b); $\mathbf{W}_h = \begin{bmatrix} 0 & 1 \\ 1 & 0 \end{bmatrix}$ in (c); $\mathbf{W}_h = \begin{bmatrix} 0 & 1.5 \\ -1.5 & 0 \end{bmatrix}$ with $\varepsilon, \gamma = 0.001$ in (d).

using this observation and the result in eq. 11. In fact, computing the spectral radius of $\mathbf{J}_F(\mathbf{0}, \mathbf{0})$ we find that:

$$\begin{aligned} \rho(\mathbf{J}_F(\mathbf{0}, \mathbf{0})) &= \max_i \sqrt{(1 - \varepsilon\gamma)^2 + \varepsilon^2 b_i^2} \\ &= \sqrt{1 + \varepsilon^2 \gamma^2 - 2\varepsilon\gamma + \varepsilon^2 \rho(\mathbf{W}_h)^2}. \end{aligned} \tag{13}$$

□

Corollary 1 clearly indicates the marginal role of the spectral radius of the recurrent weight matrix \mathbf{W}_h in determining the effective spectral radius of the EuSN, hence the asymptotic behavior of the system. The influence of $\rho(\mathbf{W}_h)$ on $\rho(\mathbf{J}_F(\mathbf{0}, \mathbf{0}))$ is indeed progressively more negligible for smaller values of the step size parameter ε . This aspect represents another crucial difference with respect to ESNs, and gives support to the initialization strategy proposed in Section 3, which does not require scaling the spectral radius of \mathbf{W}_h , and rather suggests a simpler scaling by an ω_r hyper-parameter after the random initialization.

Figure 2 provides some examples of values of the effective spectral radius of EuSN, computed considering reservoirs with $N = 100$ neurons, varying ε and γ between 10^{-10} and 10^{-1} , and for different values of ω_r varying from 0.001 to 1 (with resulting values of $\rho(\mathbf{W}_h)$ ranging from ≈ 0.015 to ≈ 15). For every configuration, the reported values are computed by averaging over 3 repetitions, following the reservoir initialization process described in Section 3. Results confirm that the effective spectral radius is restricted to values ≈ 1 in all the configurations, with a few exceptions, represented by the largest values of ε and ω_r .

We now extend our analysis to conditions that include non-zero input signals. To this end, we find it useful to consider the spectrum of (pseudo) local Lyapunov exponents (LLEs) [35, 36] of the reservoir. These quantities provide a measure of the sensitivity of the system to small perturbations of the state trajectories, characterizing the dynamical behavior locally to the state evolved over time. In particular, the maximum local Lyapunov exponent (MLLE) is a useful indicator of the regime of the reservoir dynamics [6, 37, 38]: values > 0 indicate unstable dynamics, values < 0 denote stable dynamics, while the condition of $MLLE = 0$ corresponds to a *critical* condition of transition between stability and instability, often referred to as the *edge of stability* (or the edge of chaos). In the RC literature, it has been observed that reservoir systems operating at the edge of stability develop richer dynamics and often result in higher performance in applications [39, 40, 41, 42, 43]. Studying the LLEs, here we show that the behavior of the reservoir of EuSNs is naturally biased towards such a critical regime. Specifically, in the following Proposition 2 we state that all the LLEs are confined to a neighborhood of 0.

Proposition 2. *Let us consider an EuSN whose reservoir dynamics are ruled by the state transition function in eq. 6, where both ε and γ are small positive scalars. The LLEs of the reservoir satisfy the following condition:*

$$LLE_i \approx 0 \quad i = 1, \dots, N, \tag{14}$$

hence, in particular

$$MLLE \approx 0. \tag{15}$$

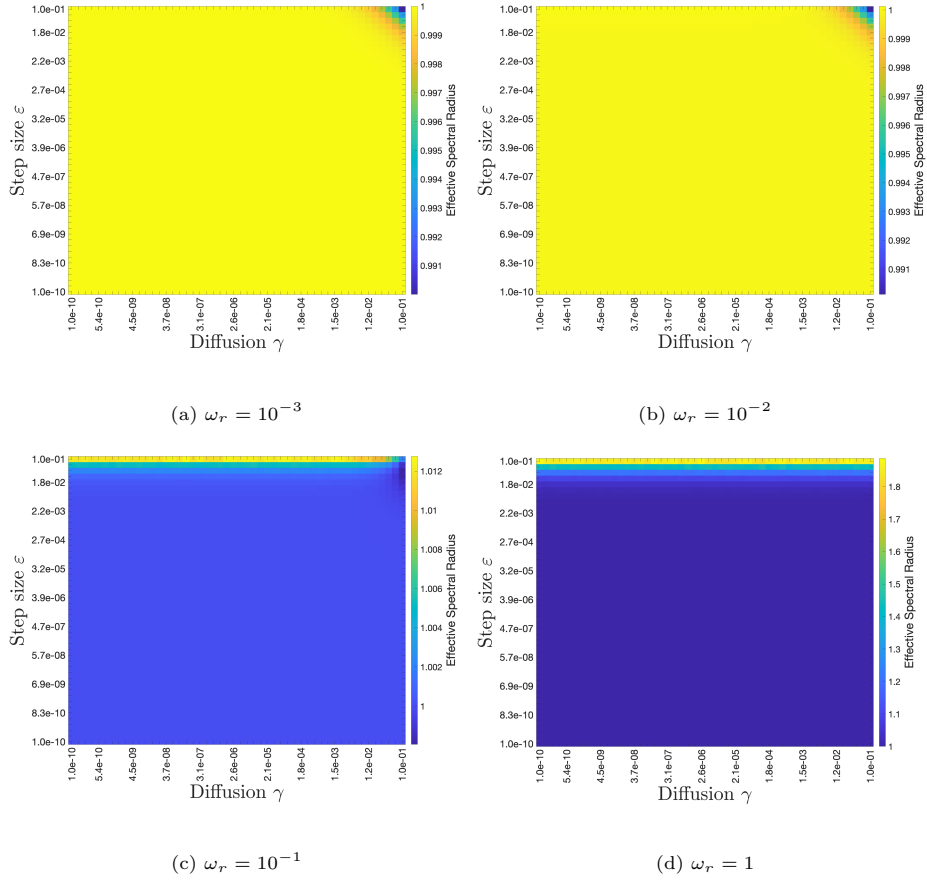


Figure 2: Effective spectral radius of EuSN with $N = 100$ reservoir neurons, for varying values of the step size (ε , vertical axis in each plot), of the diffusion (γ , horizontal axis in each plot), and of scaling of the recurrent weight matrix \mathbf{W}_h (ω_r , different plots). For each configuration, the results are averaged over 3 repetitions.

Proof. Suppose to drive the reservoir dynamics by an external time-series of length T , i.e., $\mathbf{x}(1), \dots, \mathbf{x}(T)$. To evaluate the LLEs, we consider the dynamics along the resulting state trajectory and apply the following estimator [38]:

$$LLE_i = \frac{1}{T} \sum_{t=1}^T \ln |\lambda_i(\mathbf{J}_F(\mathbf{h}(t-1), \mathbf{x}(t)))|. \quad (16)$$

Computing the full Jacobian in eq. 8, we get:

$$\mathbf{J}_F(\mathbf{h}(t-1), \mathbf{x}(t)) = \mathbf{I} + \varepsilon \mathbf{D}(t) \mathbf{W}_h - \varepsilon \gamma \mathbf{D}(t), \quad (17)$$

where $\mathbf{D}(t)$ is a diagonal matrix whose entries are given by $1 - \tilde{\mathbf{h}}_1^2(t)$, $1 - \tilde{\mathbf{h}}_2^2(t), \dots, 1 - \tilde{\mathbf{h}}_N^2(t)$, with $\tilde{\mathbf{h}}_i(t)$ denoting the i -th component of the vector $\tanh\left((\mathbf{W}_h - \gamma \mathbf{I})\mathbf{h}(t-1) + \mathbf{W}_x \mathbf{x}(t) + \mathbf{b}\right)$. Now, observing that the non-zero values in $\mathbf{D}(t)$ are restricted to the range $[0, 1]$, and recalling that ε and γ both take small positive values, we can see that the expression in right-hand side of eq. 17 is dominated by the identity matrix. Hence, similarly to the proof of Proposition 1, we can derive that the eigenvalues of the Jacobian are all restricted to values close to 1, i.e.,:

$$\lambda_i(\mathbf{J}_F(\mathbf{h}(t-1), \mathbf{x}(t))) \approx 1 \quad i = 1, \dots, N, \quad t = 1, \dots, T. \quad (18)$$

Finally, using eq. 18 in eq. 16, we can conclude that $LLE_i \approx 0$ for all $i = 1, \dots, N$, and in particular that $MLLE \approx 0$. \square

To concretely illustrate the result of Proposition 2, we numerically compute the LLEs of reservoir dynamics in EuSN with $N = 100$, using the estimator in eq. 16, and considering as driving input a one-dimensional time-series of length 500 whose elements are randomly drawn from a uniform distribution over $[-0.5, 0.5]$, with $\omega_x = \omega_b = 1$. Varying the ε , γ and ω_r hyper-parameters as in Figure 2, in Figure 3 we show the resulting MLLE (averaged over 3 repetitions for every configuration). As results clearly show, the obtained MLLE is ≈ 0 in every configuration, confirming the analytical outcomes of Proposition 2 regarding the intrinsic critical regime of EuSN dynamics.

5. Experiments

The mathematical analysis provided in Section 4 pointed out that EuSN dynamics are naturally biased towards the edge of stability. In this section, we show the relevant impact that such a characterization can have in applications. First, in Section 5.1, we analyze the impact on tasks involving long-term memorization in comparison to RC models. Then, in Section 5.2 we analyze the resulting performance (in terms of accuracy, required times, and energy consumption) on several time-series classification tasks, in comparison to both RC models and trainable RNN architectures.

The experiments described in this section were ran in single-GPU mode, on a system equipped with 2x20 Intel(R) Xeon(R) CPU E5-2698 v4 @ 2.20GHz, and 4 Tesla P100-PCIE-16GB GPU. The code used for our experiments is written in Keras and is made publicly available online².

²<https://github.com/gallicch/EulerStateNetworks>

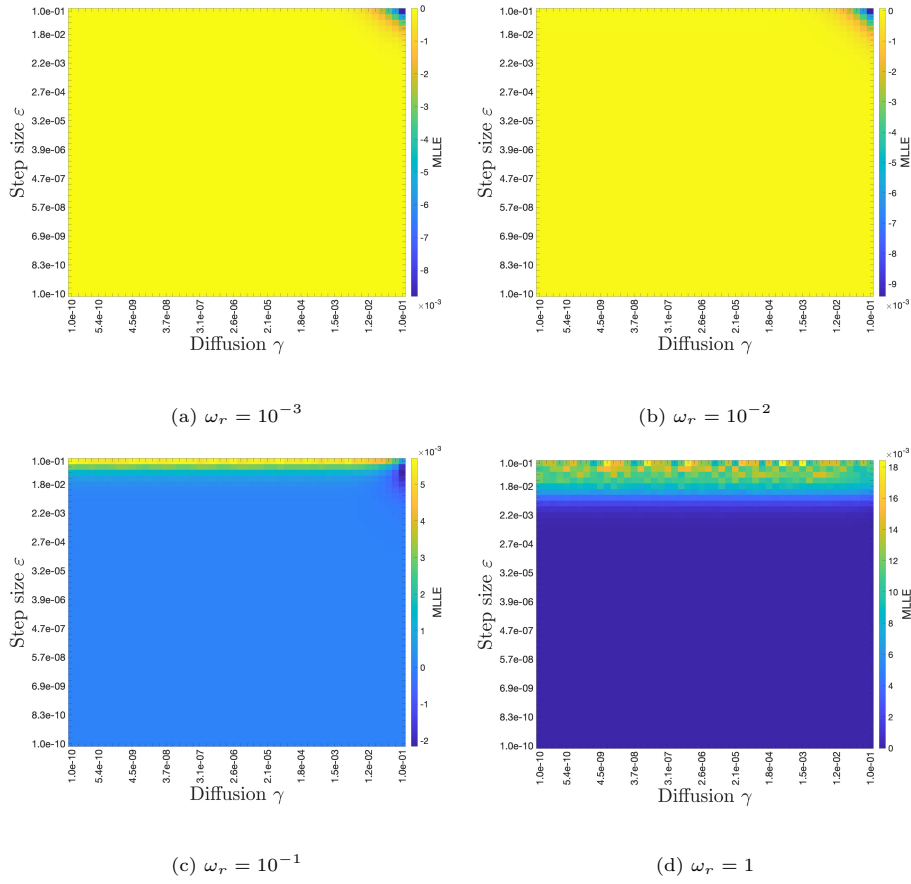


Figure 3: MLE of EuSN with $N = 100$ reservoir neurons, for varying values of the step size (ϵ , vertical axis in each plot), of the diffusion (γ , horizontal axis in each plot), and of scaling of the recurrent weight matrix \mathbf{W}_h (ω_r , different plots). For each configuration, the results are averaged over 3 repetitions. See details in the text.

5.1. Long-term Memorization

We introduce a family of time-series classification tasks to assess the long-term memorization (LTM) skills of recurrent layers. We generate 1-dimensional input time-series containing triplets of +1s or -1s with the same probability, followed by a number of τ_p random padding values drawn from a uniform distribution over $(0, 1)$. We then assign a class label of 1 to each time-series where the initial triplet contains +1s, and a class label of 0 to the others. Notice that the classification task becomes more and more challenging for increasing values of the padding length τ_p , requiring progressively longer-term memorization ability to recall the initial input information provided to the network. We considered values of τ_p ranging from 100 to 1000, and – for every choice of τ_p – we generated a dataset of 1000 time-series, equally divided (with stratification) into training set and test set. Data intended for training have been divided into a training and a validation set by a further (stratified) 50%-50% split.

Experimental Settings – We considered EuSNs with $N = 100$ reservoir neurons, exploring values of the network hyper-parameters in the following ranges: ω_r , ω_x and ω_b in $(0.01, 1.5)$ with linear sampling; ε and γ in $(10^{-5}, 10^{-1})$ with logarithmic sampling. For comparison, we ran experiments with ESNs and R-ESNs configured with the same number of reservoir neurons. In this case, we explored values of $\rho(\mathbf{W}_h)$, ω_x and ω_b in $(0.01, 1.5)$, and α in $(0.01, 1)$ with linear sampling. In all the cases, the readout was implemented by a dense layer, with sigmoid activation, fed by the last state computed by the reservoir for each time-series. The readout was trained using RMSprop, with binary cross-entropy loss, for a maximum number of 200 epochs, using early stopping with patience 10 on the validation set. The learning rate of the training algorithm η was treated as a hyper-parameter, and explored in the range $(10^{-5}, 10^{-1})$ with logarithmic sampling. The hyper-parameters were fine-tuned by model selection on the validation set using Hyperband [44], individually for each model. After model selection, for each model we generated 10 instances (random guesses) of the network with the selected configuration. The 10 instances were trained on the training set and evaluated on the test set. The reported results have been finally achieved by computing averages and standard deviations over the 10 instances.

Results – The results on the LTM tasks are reported in Figure 4, which shows the test set accuracy achieved by EuSN, ESN and R-ESN, for increasing values of the padding length τ_p . As it is visible from the plot, EuSN consistently reaches an almost perfect value of LTM accuracy, even at 1000 time-steps away from the information that is relevant to the classification. At the same time, consistent with its fading memory characterization, ESN shows a rapidly degrading performance, that is already at the level of chance (i.e., ≈ 0.5) after a few hundred time-steps. A similar trend is shown by the R-ESN variant, which initially outperforms ESN and reaches a performance close to that one of EuSN (for $\tau_p = 100$), and then also rapidly degrades at the level of chance. It is also worth noticing the small variability of EuSN results (vertical error bars in the plot), suggesting that the LTM ability is almost not affected by the randomization in the choice of the weight values. By contrast, a larger variability is observed for ESN and R-ESN.

Overall, results in Figure 4 clearly indicate that EuSN are able to propagate the input information effectively across many time-steps, overcoming the fading memory limitations which are typical of ESN variants.

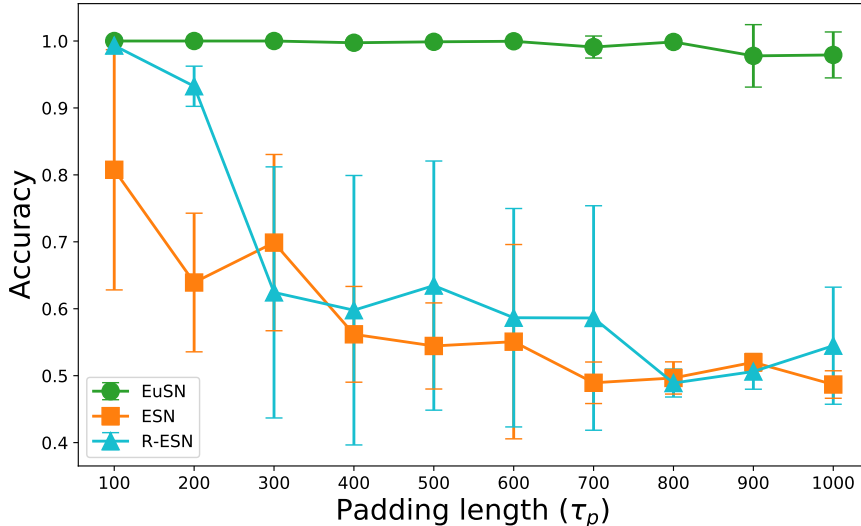


Figure 4: Accuracy achieved on the LTM tasks by EuSN for increasing length of the random padding (τ_p). Results are compared to standard ESN and R-ESN.

5.2. Time-series Classification

We assessed the performance of EuSN on several real-world time-series classification benchmarks of diverse nature. The first 10 datasets were taken from the UEA & UCR time-series classification repository [45], namely: *Adiac* [46], *CharacterTrajectories* [47], *ECG5000* [48], *Epilepsy* [49], *HandOutlines* [50], *Hearthbeat* [48], *Libras* [51], *ShapesAll* [52], *SpokenArabicDigits* [53], and *Wafer* [54]. Moreover, we have considered the *IMDB* movie review sentiment classification dataset [55], and the *Reuters* newswire classification dataset from UCI [56]. These two last datasets were utilized in the parsed version that is made publicly available online³. In addition, individually for the two tasks, we have applied a pre-processing phase to represent each sentence by a time-series of 32-dimensional word embeddings⁴. For all datasets, we have used the original data splitting into training and test, with a further stratified splitting of the original training data into training (66%) and validation (33%) sets. A summary of the relevant information for

³IMDB: <https://keras.io/api/datasets/imdb/>; Reuters: <https://keras.io/api/datasets/reuters/>

⁴Each sentence was represented by a sequence of words among the 10000 most frequent words in the database, with truncation to the maximum length of 200. Word embeddings have been obtained by training an MLP architecture with preliminary embedding layer with 32 units, a hidden layer containing 128 units with ReLU activation, and a final dense output layer (with 1 sigmoidal unit for IMDB, and 46 softmax units for Reuters). This architecture was trained on the training set with RMSProp for 100 epochs, using early stopping with patience 10 on a validation set containing the 33% of the original training data. The output of the embedding layer on the sentences in the dataset is then used as input feature for our experiments.

Name	#Seq Tr	#Seq Ts	Length	Feat.	Classes
Adiac	390	391	176	1	37
CharacterTrajectories	1422	1436	182	3	20
ECG5000	500	4500	140	1	5
Epilepsy	137	138	207	3	4
HandOutlines	1000	370	2709	1	2
Heartbeat	204	205	405	61	2
IMDB	25000	25000	200	32	2
Libras	180	180	45	2	15
Reuters	8982	2246	200	32	46
ShapesAll	600	600	512	1	60
SpokenArabicDigits	6599	2199	93	13	10
Wafer	1000	6164	152	1	2

Table 1: Information on the time-series classification benchmarks used in the paper, namely: size of the training (#Seq Tr) and of the test set (#Seq Ts), length of the time-series (Length), number of input features, i.e., input dimensionality X (Feat.), and number of class labels (Classes).

each dataset is given in Table 1.

Experimental Settings – We have run experiments with EuSNs on the above mentioned time-series classification tasks following the same base experimental setting already introduced in Section 5.1 for the LTM tasks. In this case, however, we extended the extent of the comparative analysis to a pool of trainable RNN architectures, including (vanilla) RNNs, A-RNN [32], Gated Recurrent Unit (GRU) [57] and Long Short-Term Memory (LSTM) [58]. In addition, for all models we explored architectural configurations with a number of recurrent/reservoir neurons N varying in the integer range 5–200, and treated as an additional hyper-parameter. The output (readout) layer was implemented by a dense layer with with 1 sigmoid unit for the binary classification tasks, and a number of softmax units equal to the number of target classes for multi-classification tasks. Analogously, we used binary or categorical cross-entropy as loss function during training, depending on the number of target classes. Model selection was performed individually for each model on the validation set.

In addition to the accuracy results, for every task and every model we measured the required computational times. Moreover, to evaluate the energy footprint, we measured the energy consumed for running all the experiments, integrating the power draw of the GPU (measured in W), sampled every 10 seconds using the NVIDIA System Management Interface. Notice that – differently from the other models – GRU and LSTM implementations could exploit the optimized cuDNN code available through Keras (resulting in a demand of computational resources that is far lower than that which would have resulted from a custom implementation).

Results – For the sake of cleanliness of results presentation, here we report a graphical illustration of the main results of the performed experiments. The reader can find full details on the obtained results reported in Appendix Appendix A, in Table A.2.

Figure 5 shows the test set accuracy achieved by the considered models on the time-series classification benchmarks. Figures 6, and 7, which follow a similar trend, respectively illustrate the times needed for model selection (in minutes), and the energy consumption required for running the experiments (in kWh).

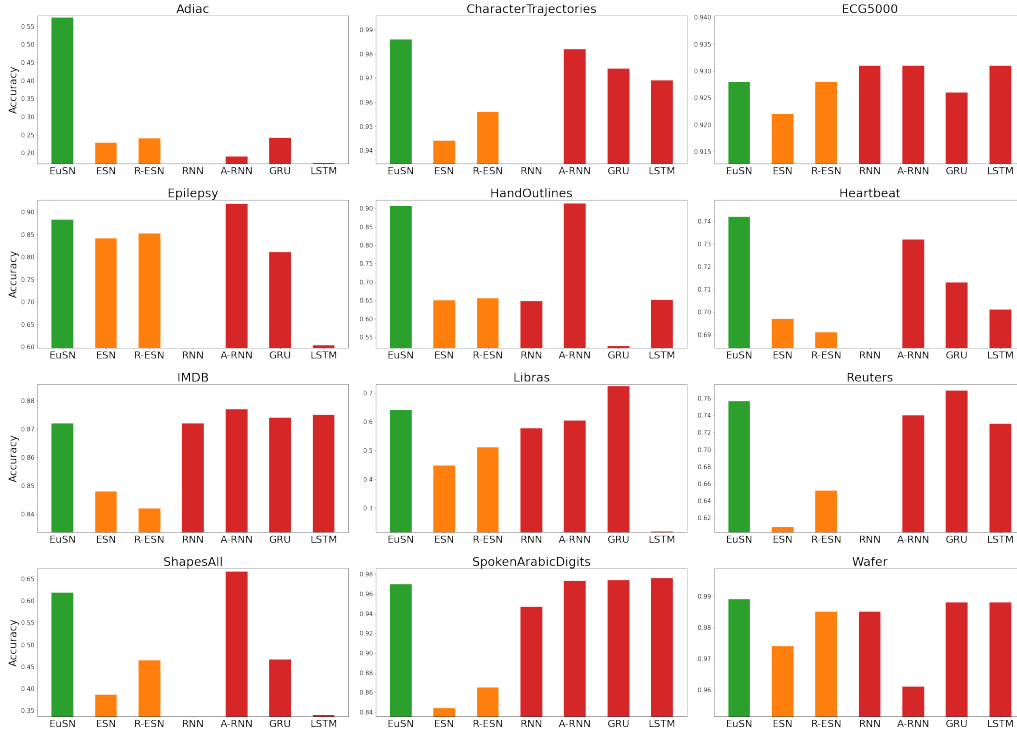


Figure 5: Test set accuracy.

Two major observations can be drawn from the results. First, from Figure 5 it is evident that EuSN consistently outperforms in terms of accuracy both ESN and R-ESN on all the tasks. Remarkably, EuSN was always able to achieve a degree of accuracy in line with (sometimes even superior to) the highest among fully trainable models, or in any case to significantly reduce the performance gap with respect to RC methods. Second, looking at Figures 6 and 7, we can see that leveraging untrained dynamics, EuSN proved to be as efficient as standard RC networks, and far more efficient than fully trainable RNNs. Overall, compared to fully trainable models, while showing high accuracy, EuSN allowed a dramatic advantage in terms of required computational resources, enabling up to a $\approx 100x$ reduction in computational times and energy consumption.

Narrowing our attention to the baseline RC models, we can also observe that the highest accuracy was obtained in most cases by the R-ESN model, thus confirming the goodness of this architectural variant against standard ESN in applications. Among the fully trained models, the highest accuracy was obtained in most cases by the A-RNN model, which, however, proved to be the least efficient overall, giving further evidence of the effectiveness of the architectural bias exploited by EuSN, while emphasizing its efficiency.

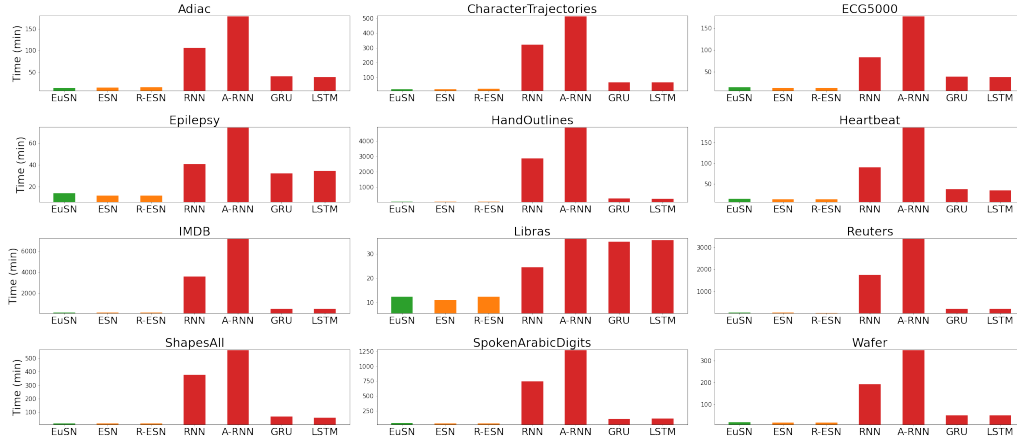


Figure 6: Time required for model selection (in minutes).

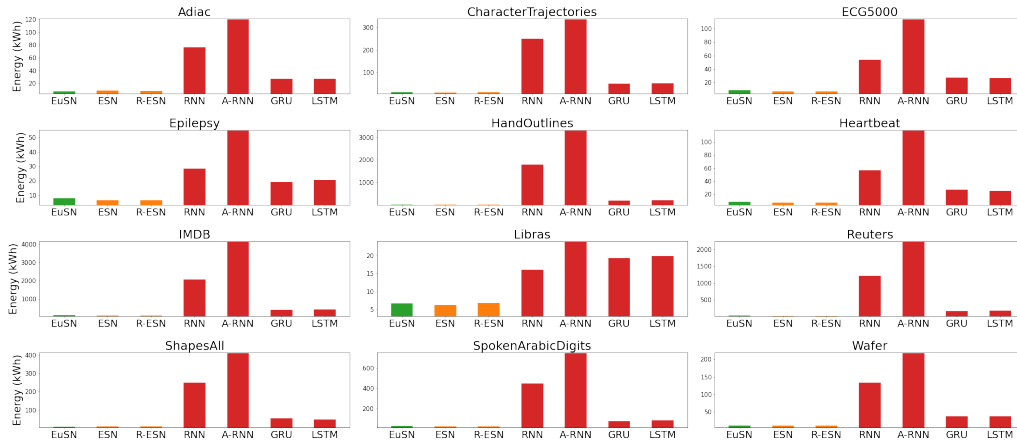


Figure 7: Energy consumption (in kWh).

6. Conclusions

In this paper we have introduced the Euler State Network (EuSN) model, a novel approach to design RC neural networks, based on the numerical discretization of ODEs by the forward Euler method. The proposed approach leverages the idea of constraining the recurrent reservoir weight matrix to have an antisymmetric structure, resulting in dynamics that are neither lossy nor unstable, and allowing for an effective transmission of input signals over time. Moreover, being featured by untrained recurrent neurons, EuSNs combine the ability to model long-term propagation of input signals with the efficiency typical of RC.

Our mathematical analysis of reservoir dynamics revealed that EuSNs are biased towards unitary effective spectral radius and zero local Lyapunov exponents, indicating an intrinsically critical dynamical regime near the edge of stability. Experiments on synthetic datasets have shown the effectiveness of EuSN in long-term memorization

of input signals, overcoming the inherent limitations of baseline RC models. Furthermore, through experiments on real-world time-series classification problems, we found that EuSN provides a formidable trade-off between accuracy and efficiency, compared to several state-of-the-art recurrent neural models. In fact, while reaching – or even outperforming – the highest level of accuracy achieved by the fully trainable models, the proposed EuSN allows up to a 100 times reduction in computation time and energy consumption.

Overall, the work presented in this paper is seminal and, as such, intends to represent only a first step in the study of ODE-inspired RC architectures and their theoretical properties. Although the presented results are already very encouraging, new directions for future works can be envisaged, for example deepening the study of the differences between ESN and EuSN in terms of reservoir state space organization and nature of the memory structure. Future work would also deserve to explore extensions to graph processing and implementations in neuromorphic hardware.

References

- [1] R. T. Chen, Y. Rubanova, J. Bettencourt, D. K. Duvenaud, Neural ordinary differential equations, *Advances in neural information processing systems* 31 (2018).
- [2] B. Chang, L. Meng, E. Haber, L. Ruthotto, D. Begert, E. Holtham, Reversible architectures for arbitrarily deep residual neural networks, in: *Proceedings of the AAAI Conference on Artificial Intelligence*, Vol. 32, 2018.
- [3] B. Chang, L. Meng, E. Haber, F. Tung, D. Begert, Multi-level residual networks from dynamical systems view, *arXiv preprint arXiv:1710.10348* (2017).
- [4] Y. Lu, A. Zhong, Q. Li, B. Dong, Beyond finite layer neural networks: Bridging deep architectures and numerical differential equations, in: *International Conference on Machine Learning*, PMLR, 2018, pp. 3276–3285.
- [5] E. Haber, L. Ruthotto, Stable architectures for deep neural networks, *Inverse Problems* 34 (1) (2017) 014004.
- [6] D. Verstraeten, B. Schrauwen, M. d’Haene, D. Stroobandt, An experimental unification of reservoir computing methods, *Neural networks* 20 (3) (2007) 391–403.
- [7] M. Lukoševičius, H. Jaeger, Reservoir computing approaches to recurrent neural network training, *Computer Science Review* 3 (3) (2009) 127–149.
- [8] M. Dragone, G. Amato, D. Bacciu, S. Chessa, S. Coleman, M. Di Rocco, C. Gallicchio, C. Gennaro, H. Lozano, L. Maguire, et al., A cognitive robotic ecology approach to self-configuring and evolving aal systems, *Engineering Applications of Artificial Intelligence* 45 (2015) 269–280.
- [9] D. Bacciu, P. Barsocchi, S. Chessa, C. Gallicchio, A. Micheli, An experimental characterization of reservoir computing in ambient assisted living applications, *Neural Computing and Applications* 24 (6) (2014) 1451–1464.
- [10] G. Tanaka, T. Yamane, J. B. Héroux, R. Nakane, N. Kanazawa, S. Takeda, H. Numata, D. Nakano, A. Hirose, Recent advances in physical reservoir computing: A review, *Neural Networks* 115 (2019) 100–123.
- [11] J. Torrejon, M. Riou, F. A. Araujo, S. Tsunegi, G. Khalsa, D. Querlioz, P. Bortolotti, V. Cros, K. Yakushiji, A. Fukushima, et al., Neuromorphic computing with nanoscale spintronic oscillators, *Nature* 547 (7664) (2017) 428–431.
- [12] D. Marković, J. Grollier, Quantum neuromorphic computing, *Applied physics letters* 117 (15) (2020) 150501.
- [13] C. Gallicchio, Reservoir computing by discretizing odes, in: *Proceedings of ESANN*, 2021.
- [14] H. Jaeger, H. Haas, Harnessing nonlinearity: Predicting chaotic systems and saving energy in wireless communication, *science* 304 (5667) (2004) 78–80.
- [15] H. Jaeger, The ”echo state” approach to analysing and training recurrent neural networks - with an erratum note, *Tech. rep.*, GMD - German National Research Institute for Computer Science (2001).
- [16] H. Jaeger, M. Lukoševičius, D. Popovici, U. Siewert, Optimization and applications of echo state networks with leaky-integrator neurons, *Neural networks* 20 (3) (2007) 335–352.

- [17] I. Yildiz, H. Jaeger, S. Kiebel, Re-visiting the echo state property, *Neural networks* 35 (2012) 1–9.
- [18] P. Verzelli, C. Alippi, L. Livi, Learn to synchronize, synchronize to learn, *Chaos: An Interdisciplinary Journal of Nonlinear Science* 31 (8) (2021) 083119.
- [19] A. Ceni, P. Ashwin, L. Livi, C. Postlethwaite, The echo index and multistability in input-driven recurrent neural networks, *Physica D: Nonlinear Phenomena* 412 (2020) 132609.
- [20] G. Manjunath, H. Jaeger, Echo state property linked to an input: Exploring a fundamental characteristic of recurrent neural networks, *Neural computation* 25 (3) (2013) 671–696.
- [21] M. Lukoševičius, A practical guide to applying echo state networks, in: *Neural networks: Tricks of the trade*, Springer, 2012, pp. 659–686.
- [22] C. Gallicchio, A. Micheli, L. Pedrelli, Fast spectral radius initialization for recurrent neural networks, in: *INNS Big Data and Deep Learning conference*, Springer, 2019, pp. 380–390.
- [23] C. Gallicchio, A. Micheli, Architectural and markovian factors of echo state networks, *Neural Networks* 24 (5) (2011) 440–456.
- [24] P. Tiño, B. Hammer, M. Bodén, Markovian bias of neural-based architectures with feedback connections, in: *Perspectives of neural-symbolic integration*, Springer, 2007, pp. 95–133.
- [25] B. Hammer, P. Tiño, Recurrent neural networks with small weights implement definite memory machines, *Neural Computation* 15 (8) (2003) 1897–1929.
- [26] T. Strauss, W. Wustlich, R. Labahn, Design strategies for weight matrices of echo state networks, *Neural computation* 24 (12) (2012) 3246–3276.
- [27] O. L. White, D. D. Lee, H. Sompolinsky, Short-term memory in orthogonal neural networks, *Physical review letters* 92 (14) (2004) 148102.
- [28] M. Henaff, A. Szlam, Y. LeCun, Recurrent orthogonal networks and long-memory tasks, in: *International Conference on Machine Learning*, PMLR, 2016, pp. 2034–2042.
- [29] P. Verzelli, C. Alippi, L. Livi, P. Tino, Input representation in recurrent neural networks dynamics, *arXiv preprint arXiv:2003.10585* (2020).
- [30] P. Tino, Dynamical systems as temporal feature spaces., *J. Mach. Learn. Res.* 21 (2020) 44–1.
- [31] A. Rodan, P. Tiño, Minimum complexity echo state network, *IEEE transactions on neural networks* 22 (1) (2010) 131–144.
- [32] B. Chang, M. Chen, E. Haber, E. H. Chi, Antisymmetricrnn: A dynamical system view on recurrent neural networks, *arXiv preprint arXiv:1902.09689* (2019).
- [33] E. Süli, D. F. Mayers, *An introduction to numerical analysis*, Cambridge university press, 2003.
- [34] C. Gallicchio, S. Scardapane, Deep randomized neural networks, *Recent Trends in Learning From Data* (2020) 43–68.
- [35] B. Bailey, *Local lyapunov exponents: predictability depends on where you are*, *Nonlinear Dynamics and Economics*, Cambridge University Press (1996) 345–359.
- [36] H. D. Abarbanel, R. Brown, M. B. Kennel, Local lyapunov exponents computed from observed data, *Journal of Nonlinear Science* 2 (3) (1992) 343–365.
- [37] D. Verstraeten, B. Schrauwen, On the quantification of dynamics in reservoir computing, in: *International Conference on Artificial Neural Networks*, Springer, 2009, pp. 985–994.
- [38] F. Bianchi, L. Livi, C. Alippi, Investigating echo state networks dynamics by means of recurrence analysis, *arXiv preprint arXiv:1601.07381* (2016) 1–25.
- [39] C. Gallicchio, A. Micheli, L. Silvestri, Local lyapunov exponents of deep echo state networks, *Neurocomputing(Accepted)* (2017).
- [40] R. Legenstein, W. Maass, Edge of chaos and prediction of computational performance for neural circuit models, *Neural networks* 20 (3) (2007) 323–334.
- [41] R. Legenstein, W. Maass, What makes a dynamical system computationally powerful, *New directions in statistical signal processing: From systems to brain* (2007) 127–154.
- [42] N. Bertschinger, T. Natschläger, Real-time computation at the edge of chaos in recurrent neural networks, *Neural computation* 16 (7) (2004) 1413–1436.
- [43] J. Boedecker, O. Obst, J. Lizier, N. Mayer, M. Asada, Information processing in echo state networks at the edge of chaos, *Theory in Biosciences* 131 (3) (2012) 205–213.
- [44] L. Li, K. Jamieson, G. DeSalvo, A. Rostamizadeh, A. Talwalkar, Hyperband: A novel bandit-based approach to hyperparameter optimization, *The Journal of Machine Learning Research* 18 (1) (2017) 6765–6816.
- [45] A. Bagnall, J. L. W. Vickers, E. Keogh, The uea & ucr time series classification repository, www.timeseriesclassification.com.
- [46] A. C. Jalba, M. H. Wilkinson, J. B. Roerdink, Automatic segmentation of diatom images for classification, *Microscopy research and technique* 65 (1-2) (2004) 72–85.
- [47] B. H. Williams, M. Toussaint, A. J. Storkey, Extracting motion primitives from natural handwriting

- data, in: International Conference on Artificial Neural Networks, Springer, 2006, pp. 634–643.
- [48] A. L. Goldberger, L. A. Amaral, L. Glass, J. M. Hausdorff, P. C. Ivanov, R. G. Mark, J. E. Mietus, G. B. Moody, C.-K. Peng, H. E. Stanley, Physiobank, physiotookit, and physionet: components of a new research resource for complex physiologic signals, *circulation* 101 (23) (2000) e215–e220.
- [49] J. R. Villar, P. Vergara, M. Menéndez, E. de la Cal, V. M. González, J. Sedano, Generalized models for the classification of abnormal movements in daily life and its applicability to epilepsy convulsion recognition, *International journal of neural systems* 26 (06) (2016) 1650037.
- [50] L. M. Davis, B.-J. Theobald, J. Lines, A. Toms, A. Bagnall, On the segmentation and classification of hand radiographs, *International journal of neural systems* 22 (05) (2012) 1250020.
- [51] D. B. Dias, R. C. Madeo, T. Rocha, H. H. Biscaro, S. M. Peres, Hand movement recognition for brazilian sign language: a study using distance-based neural networks, in: 2009 international joint conference on neural networks, IEEE, 2009, pp. 697–704.
- [52] L. J. Latecki, R. Lakamper, T. Eckhardt, Shape descriptors for non-rigid shapes with a single closed contour, in: Proceedings IEEE Conference on Computer Vision and Pattern Recognition. CVPR 2000 (Cat. No. PR00662), Vol. 1, IEEE, 2000, pp. 424–429.
- [53] N. Hammami, M. Bedda, Improved tree model for arabic speech recognition, in: 2010 3rd International Conference on Computer Science and Information Technology, Vol. 5, IEEE, 2010, pp. 521–526.
- [54] R. T. Olszewski, Generalized feature extraction for structural pattern recognition in time-series data, Carnegie Mellon University, 2001.
- [55] A. L. Maas, R. E. Daly, P. T. Pham, D. Huang, A. Y. Ng, C. Potts, Learning word vectors for sentiment analysis, in: Proceedings of the 49th Annual Meeting of the Association for Computational Linguistics: Human Language Technologies, Association for Computational Linguistics, Portland, Oregon, USA, 2011, pp. 142–150.
URL <http://www.aclweb.org/anthology/P11-1015>
- [56] C. Apté, F. Damerau, S. M. Weiss, Automated learning of decision rules for text categorization, *ACM Transactions on Information Systems (TOIS)* 12 (3) (1994) 233–251.
- [57] J. Chung, C. Gulcehre, K. Cho, Y. Bengio, Empirical evaluation of gated recurrent neural networks on sequence modeling, arXiv preprint arXiv:1412.3555 (2014).
- [58] S. Hochreiter, J. Schmidhuber, Long short-term memory, *Neural computation* 9 (8) (1997) 1735–1780.

Appendix A. Detailed Results

Here, in Table A.2, we report the full details of the experimental outcomes on the time-series classification datasets described in Section 5.

For every task and for every model, results in Table A.2 include the test set accuracy (averaged over the 10 random guesses, and indicating the standard deviations), the number of trainable parameters of the selected configuration, the time required for training and testing the selected configuration (averaged over the 10 random guesses, and indicating the standard deviations), the time required for model selection, and the energy consumed to perform all the experiments. Besides the considerations already made in Section 5, the accuracy results in the table also show a consistently smaller standard deviation of EuSN, in comparison to ESN and R-ESN.

Adiac						
	<i>Acc</i>	<i># Par</i>	<i>Time (min.)</i>	<i>MS Time (min.)</i>	<i>Energy (kWh)</i>	
EuSN (ours)	0.574 (± 0.034)	6512	0.072 (± 0.006)	13.445	7.459	
ESN	0.228 (± 0.045)	4033	0.197 (± 0.004)	14.369	8.630	
R-ESN	0.240 (± 0.048)	7363	0.076 (± 0.031)	14.703	8.086	
RNN	0.164 (± 0.043)	34813	2.468 (± 1.082)	105.303	76.339	
A-RNN	0.190 (± 0.033)	39457	2.617 (± 0.837)	178.669	120.167	
GRU	0.242 (± 0.076)	4822	0.293 (± 0.067)	40.110	27.306	
LSTM	0.172 (± 0.054)	143741	0.296 (± 0.096)	38.502	26.789	
CharacterTrajectories						
	<i>Acc</i>	<i># Par</i>	<i>Time (min.)</i>	<i>MS Time (min.)</i>	<i>Energy (kWh)</i>	
EuSN (ours)	0.986 (± 0.002)	3960	0.115 (± 0.013)	19.454	11.909	
ESN	0.944 (± 0.016)	4033	0.116 (± 0.015)	18.359	11.249	
R-ESN	0.956 (± 0.008)	3520	0.123 (± 0.015)	20.796	12.768	
RNN	0.792 (± 0.024)	21780	10.650 (± 2.356)	319.960	250.433	
A-RNN	0.982 (± 0.003)	5652	4.706 (± 0.687)	512.507	336.350	
GRU	0.974 (± 0.007)	80442	0.639 (± 0.159)	65.214	50.202	
LSTM	0.969 (± 0.010)	130260	0.560 (± 0.065)	66.693	52.033	
ECG5000						
	<i>Acc</i>	<i># Par</i>	<i>Time (min.)</i>	<i>MS Time (min.)</i>	<i>Energy (kWh)</i>	
EuSN (ours)	0.928 (± 0.002)	620	0.071 (± 0.007)	14.328	8.623	
ESN	0.922 (± 0.005)	995	0.049 (± 0.007)	12.072	7.179	
R-ESN	0.928 (± 0.003)	760	0.051 (± 0.010)	11.914	7.185	
RNN	0.931 (± 0.003)	20015	0.842 (± 0.178)	83.282	53.622	
A-RNN	0.931 (± 0.003)	545	1.763 (± 0.316)	177.369	113.835	
GRU	0.926 (± 0.009)	117997	0.174 (± 0.021)	38.720	27.441	
LSTM	0.931 (± 0.002)	100642	0.187 (± 0.018)	37.904	26.918	
Epilepsy						
	<i>Acc</i>	<i># Par</i>	<i>Time (min.)</i>	<i>MS Time (min.)</i>	<i>Energy (kWh)</i>	
EuSN (ours)	0.883 (± 0.015)	252	0.107 (± 0.017)	14.035	7.985	
ESN	0.842 (± 0.042)	704	0.042 (± 0.004)	11.795	6.391	
R-ESN	0.853 (± 0.034)	704	0.045 (± 0.012)	11.849	6.480	
RNN	0.518 (± 0.075)	18484	0.815 (± 0.200)	40.716	28.453	
A-RNN	0.918 (± 0.007)	15117	1.968 (± 0.085)	74.168	54.780	
GRU	0.811 (± 0.046)	1584	0.136 (± 0.010)	32.048	19.210	
LSTM	0.604 (± 0.040)	12748	0.149 (± 0.017)	34.484	20.407	
HandOutlines						
	<i>Acc</i>	<i># Par</i>	<i>Time (min.)</i>	<i>MS Time (min.)</i>	<i>Energy (kWh)</i>	
EuSN (ours)	0.907 (± 0.005)	93	0.296 (± 0.025)	37.941	22.317	
ESN	0.650 (± 0.007)	199	0.295 (± 0.006)	35.325	20.952	
R-ESN	0.656 (± 0.007)	199	0.277 (± 0.020)	36.555	21.859	
RNN	0.648 (± 0.011)	701	21.052 (± 11.042)	2854.174	1798.302	
A-RNN	0.914 (± 0.003)	4289	70.084 (± 14.746)	4864.294	3295.017	
GRU	0.526 (± 0.136)	112513	0.877 (± 0.269)	259.611	197.604	
LSTM	0.651 (± 0.012)	134135	5.613 (± 1.428)	220.552	223.149	

Continued on next page.

Heartbeat						
	<i>Acc</i>	<i># Par</i>	<i>Time (min.)</i>	<i>MS Time (min.)</i>	<i>Energy (kWh)</i>	
EuSN (ours)	0.742 (± 0.014)	138	0.046 (± 0.005)	14.061	8.410	
ESN	0.697 (± 0.017)	176	0.053 (± 0.006)	12.302	7.375	
R-ESN	0.691 (± 0.016)	176	0.051 (± 0.005)	12.604	7.460	
RNN	0.657 (± 0.025)	3169	0.685 (± 0.157)	90.277	56.819	
A-RNN	0.732 (± 0.021)	6665	1.338 (± 0.308)	186.248	117.256	
GRU	0.713 (± 0.030)	9929	0.160 (± 0.038)	37.412	26.983	
LSTM	0.701 (± 0.016)	195265	0.162 (± 0.034)	34.265	25.249	
IMDB						
	<i>Acc</i>	<i># Par</i>	<i>Time (min.)</i>	<i>MS Time (min.)</i>	<i>Energy (kWh)</i>	
EuSN (ours)	0.872 (± 0.002)	192	1.191 (± 0.231)	151.200	99.220	
ESN	0.848 (± 0.006)	176	0.750 (± 0.223)	130.569	84.886	
R-ESN	0.842 (± 0.018)	176	0.951 (± 0.341)	130.365	86.335	
RNN	0.872 (± 0.003)	30688	24.089 (± 2.085)	3574.505	2064.461	
A-RNN	0.877 (± 0.000)	16873	43.232 (± 0.577)	7165.713	4125.985	
GRU	0.874 (± 0.004)	49169	1.921 (± 0.048)	478.161	393.846	
LSTM	0.875 (± 0.002)	116716	4.123 (± 0.578)	467.646	410.222	
Libras						
	<i>Acc</i>	<i># Par</i>	<i>Time (min.)</i>	<i>MS Time (min.)</i>	<i>Energy (kWh)</i>	
EuSN (ours)	0.642 (± 0.022)	2505	0.037 (± 0.001)	12.279	6.650	
ESN	0.448 (± 0.048)	2985	0.080 (± 0.007)	10.972	6.211	
R-ESN	0.512 (± 0.064)	2985	0.074 (± 0.010)	12.228	6.829	
RNN	0.578 (± 0.039)	33058	0.329 (± 0.068)	24.509	16.034	
A-RNN	0.604 (± 0.020)	9150	0.485 (± 0.051)	36.067	23.805	
GRU	0.724 (± 0.047)	5631	0.141 (± 0.007)	35.010	19.363	
LSTM	0.218 (± 0.233)	140407	0.130 (± 0.039)	35.615	19.852	
Reuters						
	<i>Acc</i>	<i># Par</i>	<i>Time (min.)</i>	<i>MS Time (min.)</i>	<i>Energy (kWh)</i>	
EuSN (ours)	0.757 (± 0.004)	4968	1.088 (± 0.224)	56.115	36.123	
ESN	0.609 (± 0.032)	8096	0.222 (± 0.039)	44.816	25.229	
R-ESN	0.652 (± 0.007)	6762	0.493 (± 0.083)	42.325	25.648	
RNN	0.541 (± 0.066)	27898	31.582 (± 11.063)	1747.426	1212.783	
A-RNN	0.740 (± 0.002)	54892	37.831 (± 0.921)	3374.364	2223.273	
GRU	0.769 (± 0.007)	15854	1.026 (± 0.240)	219.680	165.685	
LSTM	0.730 (± 0.010)	29218	2.111 (± 0.271)	213.727	173.522	
ShapesAll						
	<i>Acc</i>	<i># Par</i>	<i>Time (min.)</i>	<i>MS Time (min.)</i>	<i>Energy (kWh)</i>	
EuSN (ours)	0.619 (± 0.013)	10920	0.067 (± 0.003)	15.774	9.432	
ESN	0.386 (± 0.068)	10560	0.081 (± 0.015)	17.488	10.617	
R-ESN	0.465 (± 0.050)	10560	0.071 (± 0.008)	17.269	10.404	
RNN	0.215 (± 0.029)	41535	5.018 (± 1.589)	375.855	250.102	
A-RNN	0.667 (± 0.022)	21599	9.847 (± 0.986)	559.472	410.274	
GRU	0.466 (± 0.046)	36294	0.787 (± 0.071)	67.447	54.633	
LSTM	0.340 (± 0.052)	46860	0.520 (± 0.117)	59.437	48.544	

Continued on next page.

SpokenArabicDigits						
	<i>Acc</i>	<i># Par</i>	<i>Time (min.)</i>	<i>MS Time (min.)</i>	<i>Energy (kWh)</i>	
EuSN (ours)	0.970 (± 0.003)	1910	0.496 (± 0.1103)	43.027	26.899	
ESN	0.844 (± 0.026)	1760	0.270 (± 0.082)	36.685	22.209	
R-ESN	0.865 (± 0.016)	1760	0.3357 (± 0.095)	36.761	22.441	
RNN	0.947 (± 0.006)	34835	8.410 (± 2.211)	745.928	448.137	
A-RNN	0.973 (± 0.003)	9667	12.136 (± 0.909)	1269.275	749.441	
GRU	0.974 (± 0.004)	116382	0.854 (± 0.174)	111.630	75.743	
LSTM	0.976 (± 0.003)	126830	0.964 (± 0.239)	117.363	81.556	

Wafer						
	<i>Acc</i>	<i># Par</i>	<i>Time (min.)</i>	<i>MS Time (min.)</i>	<i>Energy (kWh)</i>	
EuSN (ours)	0.989 (± 0.002)	124	0.174 (± 0.0438)	17.962	11.316	
ESN	0.974 (± 0.018)	199	0.297 (± 0.078)	16.320	11.076	
R-ESN	0.985 (± 0.004)	70	0.229 (± 0.061)	16.213	10.644	
RNN	0.985 (± 0.010)	18905	3.514 (± 1.143)	192.208	133.015	
A-RNN	0.961 (± 0.018)	24179	2.446 (± 1.159)	347.315	217.542	
GRU	0.988 (± 0.002)	11401	0.364 (± 0.039)	50.718	37.532	
LSTM	0.988 (± 0.005)	97496	0.399 (± 0.119)	49.437	37.579	

Table A.2: Results on time-series classification problems achieved by EuSN, compared to ESN, R-ESN, vanilla RNN, A-RNN, GRU, and LSTM. For every dataset we report the accuracy on the test set (*Acc*), the number of trainable parameters (*#Par*), the time (in minutes) for training and test (*Time*), and for the whole model selection (*MS Time*). The last column reports the estimated Energy consumption required for all the experiments with the corresponding model (in kWh). *Acc* and *Time* indicate the average and standard deviation over the 10 random guesses.